Profile control by local ECRH in LHD

S. Kubo 1), T. Shimozuma 1), Y. Yoshimura 1), H. Igami 1), T. Notake 2), H. Takahashi 1), T. Mutoh 1), H. Tanaka 3), S. Inagaki 4), K. Tanaka 1), Y. Nagayama 1), I. Yamada 1), K. Narihara 1), S. Sakakibara 1), S. Muto 1), T. Tokuzawa 1), K. Ida 1), T. Ido 1), A. Shimizu 1), K.Y. Watanabe 1), K. Kawahata 1), N. Ohyabu 1), O. Kaneko 1), H. Yamada 1), A. Komori 1), S. Sudo 1), O. Motojima and LHD experimental group

1) National Institute for Fusion Science , Toki, Japan
2) Research Center for Development of FIR Region, Univ. of Fukui, Fukui, Japan
3) Graduate School of Energy Science, Kyoto University, Kyoto, Japan
4) Research Institute of Applied Mechanics, Kyusyu Univ., Kasuga, Japan
E-mail: kubo@LHD.nifs.ac.jp

1 Introduction

The specific and the important feature of electron cyclotron resonance heating (ECRH) in magnetic fusion experiments is the well defined deposition profile and its controllability. This feature is realized and utilized for the electron temperature profile control, investigating the transport properties and current profile control in LHD. Temporally and spatially high resolution diagnostics, motional Stark effect (MSE), heavy ion beam probe (HIBP) as well as Thomson scattering, electron cyclotron emission (ECE) are applied to such locally heated or current driven plasma in LHD. The relations between the ECRH induced flux or current and the formation of the potential and density or induced current profile structure are clearly shown experimentally for the first time. These detailed diagnostics confirmed that the ECRH power deposition profile is well localized and controlled by steering the antenna and adjusting the magnetic field configuration. The experimental set up with the verification of the beam alignment procedure is described in section2 . In relation to the deposition profile, the high energy electrons production and its effect on the deposition profile is discussed in section3. As an application of local power deposition, density profile control experiment (section 4) current profile control experient (section 5) are described followed by conclusions.

2 Experimental setup and ECRH beam confirmation

ECRH system in LHD has been operated and upgraded at 82.7, 84 GHz and 168 GHz to inject maximum injection power of more than 2 MW in total. This ECRH system in LHD is applied to the plasma profile control including electron temperature, density, potential and toroidal current. All injection system utilize the strong focusing Gaussian optics and fine controlled steering mirrors to realize local high power density electron heating in LHD. It is important to establish the method to confirm and control the power deposition profile in any ECRH applications those assume sharp and well controlled power depositions. Local high power density of more than few hundreds of MW/m^3 is confirmed and enabled to sustain high electron temperature of more than 10 keV at the center and local density, potential and current profile control have been performed[1, 2].

Direct beam profile measurements inside LHD vacuum vessel demonstrated that the injection beam from each antenna are well focused as designed and well controlled by the mirror steering

system. The antenna beam alignments and its controllability are the keys for the physics experiment. All the antennas installed in the LHD are designed to focus the injection beams and control the injection angle so that the power deposition profile is controlled depending on the experimental purposes. The antenna mirror systems are designed using the Gaussian optics code. Antenna performances were checked with low power source before installation on LHD. The alignments of the mirror setting were checked only by He-Ne laser after installation on LHD. In order to confirm the hot beam performance inside the LHD vacuum vessel, beam patten measurements and injection angle controllabilities are checked. The beam pattern measurements have been performed with thermal paper or liquid crystal plates outside of the vacuum vessel, so far, since they easily give direct information on the required position. A new method adopts infra-red camera measuring the temperature rise of a Kapton sheet target set inside the vacuum vessel. The Kapton is adopted due to several preferable characteristics for measuring beam pattern in side vacuum vessel. Adequate absorption for microwave is required to measure the beam profile from temperature rise, but not burned out even with focused high power beam. Good emissivity for infra-red region, adequate thermal capacity and conductivity are also necessary for the precise estimation of the beam pattern. In addition, unflamable and dust free natures are especially important for in vessel measurement. Reference lines and ticks is formed by weaving a thin nichrome thread on the screen. These were utilized to correct and calibrate the viewing angle distortion of the infra-red images. In such a way, the method of high power beam measurement in the vacuum vessel is established and the beam quality, alignment and its controllability are confirmed inside the vacuum vessel for almost all ECRH antenna. Figure 1 is the photo showing the measuring configuration of the beam from U-port antenna.

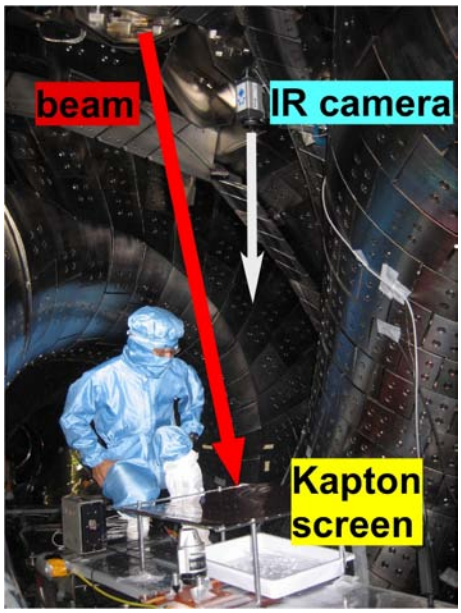

Figure 1: *Photo showing the configuration of the beam patten measurement inside LHD vacuum vessel. Taraget screen of Kapton is placed on the mid-plane of the LHD.*

The power deposition profile by ECRH in LHD is well defined estimated by the direct beam measurement inside LHD and the power modulation analysis[3]. Experimentally deduced power deposition profile well agree with the result from ray tracing calculation.

3 High energy electrons

The generation of supra-thermal electrons can alter the power deposition profile by the change of absorption mechanism and the resultant supra-thermal electrons can drift out to broaden the power deposition profile by relaxing its energy at the other flux surfaces than that where the power directly absorbed[3]. In order to clarify the generation mechanism of the supra-thermal electrons and their interaction with ECRH, second and higher harmonics ECE are calculated and compared with the experiment.

The spectrum of electron cyclotron emission (ECE) is used to estimate the bulk electron temperature for optically thick plasma, but they are sensitive to the supra-thermal electrons due to

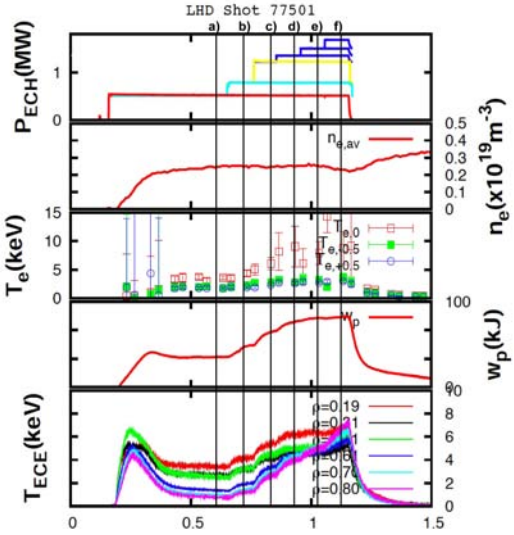

Figure 2: *Time evolutions of stored energy, electron density and radiation during low density, high power ECRH experiment.*

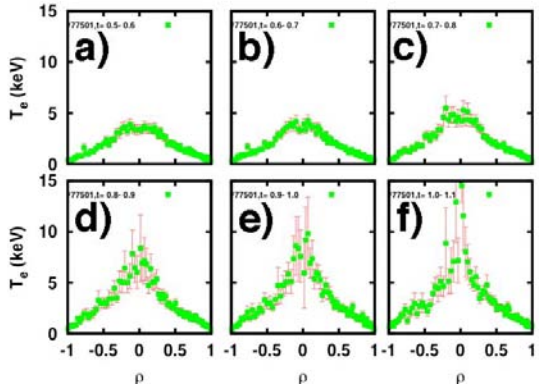

Figure 3: *T_e profiles at time slices indicated by arrows in the left figure.*

relativistic shift of the cyclotron frequency and non-thermal emission, in particular at optically thin frequency region. High power electron cyclotron resonance heating (ECRH) is a powerful tool to control the local electron pressure and current, but heating and current drive themselves rely on the deformation of the electron velocity distribution function and can generate suprathermal electrons.

The production and its thermalization of non-thermal electrons also affects the power deposition profile and might be the reason why the high temperature states is not stable. Non-thermal electrons are intensionally produced by further reducing the electron density below 2×10^{18} m^{-3}. The profile of the non-thermal electrons and energy are estimated from ECE non-thermal emission, soft and hard X ray pulse height analysis. The presence of such high energy electrons can broaden the power deposition profile and can affect the stable sustainment of the high electron temperature states.

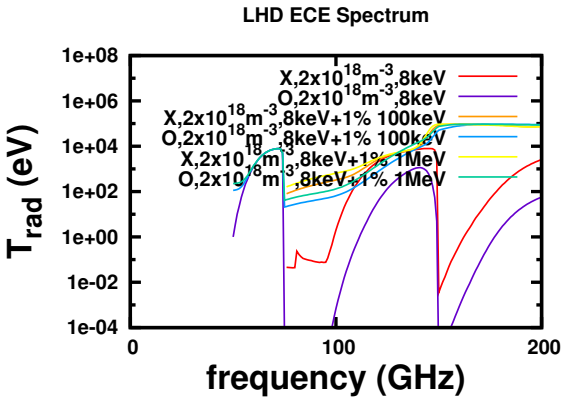

Figure 4: *Example of ECE spectrum calculation for bulk $n_e = 2 \times 10^{18}$ m^{-3}, $T_{e,0} = 8$ keV, 0.01% high energy*

High power ECRH experiments have been performed on relatively low density ($n_e \leq 0.3 \times 10^{19}$ m^{-3}) with total input power of 1.8 MW. Typical discharge waveform are shown in Fig.2. ECRH power from 1-77 GHz, 1-84 GHz, 2-82.7 GHz and 3-168 GHz is injected to LHD stepwise successively to attain 1.8 MW in total. the density is adjusted to keep $n_e \leq 0.3 \times 10^{19}$ m^{-3} as shown in the second column. Stored energy increases almost in proportional with power ant attains 80 kJ. Central electron temperature reaches 10 keV at the power level of

1 MW, but saturates or scatters at more than 1MW. Electron temperature profiles at each power level measured are shown in Fig.3 . These profiles, especially at the last two time slices shows data scattering feature near the magnetic axis. In the bottom column of Fig.2 are shown the ECE radiation temperature evolutions at ρ = 0.2, 0.3, 0.5, 0.6, 0.7, 0.8. The peripheral channels (ρ=0.7 and 0.8) clearly shows non-thermal feature at more than 1 MW power level. Hard X-ray pulse height analysis (PHA) along several vertical chords are performed simultaneously. The X-rays at energy range up to 100 keV are observed toward the end of the discharge, just as the grows of the ECE at the peripheral channels. The change of the ECE spectrum is compared with the simulated one by assuming the supra-thermal electrons derived from Hard X-ray PHA. ECE spectrum calculation solving radiation transfer equation along the line of sight shows [4, 5].

The change in ECE spectra due to the presence of high energy electrons at optically thick frequency is small due to re-absorption as shown in Fig.4. The change in ECE spectra is more sensitive at optically gray or thin frequency which corresponds to the 2nd harmonic electron cyclotron at plasma peripheral region. Measured and calculated ECE spectra shows in good correspondence assuming the high energy electron of 100 keV and 0.01-0.1 % of bulk electron density.

These results indicated that the ECE spectra measurement is sensitive to the presence of high energy electrons, but re-absorption mechanism suppress the non-thermal emission at optically thick region. Taking into account of the HX, SX pulse height analysis result, the power deposition profile is not so much disturbed by the presence and production of the high energy electrons up to the present power level and density. These behavior of high energy electrons might become critical under the more higher power density ECRH experiment in the future.

4 Density profile control

The localization of the power deposition profile can also applied to the local control of the density profile as a synergetic effect with radial electric field. The density profile response to the second harmonic ECRH at ripple top and bottom is applied to the NBI target plasma. Second harmonic ECRH at ripple bottom is expected to enhance direct radial electron flux. This direct flux can trigger radial electric filed transition as a result.

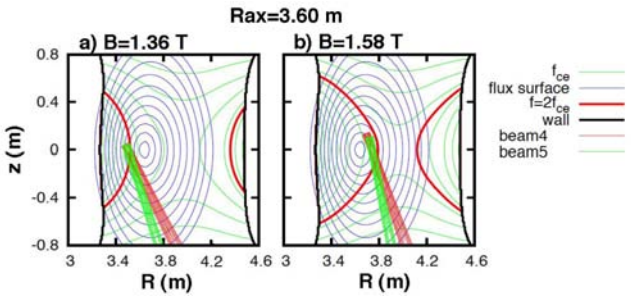

Figure 5: Vertically elongated cross section of Mod-B, flux surfaces, second harmonic resonance layers and ECRH beams for ripple a) top and b) bottom heating geometries. for R_{ax} = 3.60 m.

Density clamping or pump out is the common phenomena in tokamaks and helical systems during high power density heating, in particular electron cyclotron resonance heating. These phenomena are discussed in terms of the enhanced electron diffusion induced by the perpendicular acceleration in velocity space and the resultant electric field [7, 8, 9]. It is also pointed out that the change in the electron temperature profile can enhance radial flux due to a non zero off-diagonal term in the transport matrix which can be appreciable by the excitation of turbulent instabilities like trapped electron modes[10]. If the change of the particle flux and the resultant electric field can be localized by

the local heating of ECRH, it can be a powerful knob for the control of the particle as well as the heat transport. In order to distinguish the effect of enhanced electron flux directly driven by the ECRH or enhanced diffusion due to the change in the electron temperature or off-diagonal transport matrix, series of experiments are performed. High power density local second harmonic X (X2) mode ECRH is applied to NBI target plasma at ripple top or bottom resonance for the different ripple conditions. The difference in the transient behavior of density profile is observed between top and bottom heating, or high and low ripple configurations. X2 mode is selected because the perpendicular acceleration is more enhanced in X2 than in fundamental O mdoe (O1) mode. The role and the mechanism of ECRH induced particle flux in the particle and heat transport is discussed based on these phenomena. Such degradation of particle confinement is also observed in a tangential negative ion neutral beam (N-NB) heated plasma in LHD for low density discharges, where the electron heating is dominant but heating in parallel to the magnetic field. Such observations also support the enhancement of the off-diagonal transport term. In order to distinguish both effects, series of experiments are performd.

High power density second harmonic local ECRH is applied on the ripple top or bottom resonance position where the width of the loss cone is wider for bottom than that for top, but expected power deposition profile is identical to each other in LHD. In order to enhance the difference in the electron flux by ECRH, the heating positions and magnetic field strength are selected so that the toroidal ripple top and bottom are heated but keeping the identical normalized radial position on the same vertically elongated cross section. Figure 5 are shown the vertically elongated cross section of LHD with the Gaussian beams from bottom for the magnetic field strength of a) 1.36 T and b) 1.58 T for the R_{ax} = 3.60 m configuration. The second harmonic resonance layer is also shown in thick red lines. Strong interactions are expected at the cross section between the injected beam and the resonance. The power deposition profiles estimated from the multi-raytracing code are confirmed to be identical and sharp at normalized minor radius, ρ=0.3, for both cases.

In order to confirm the ECRH clamping effect due to the ripple and bottom heating, similar experiments with another ripple condition are tried by changing the magnetic axis position, R_{ax}. The ripple ratio is 0.15 and 0.1 for the case of R_{ax} = 3.60 and 3.75 m at normalized minor radius, ρ = 0.3, where the X2 power is equivalently focused at ripple top and bottom condition. The increases in the electron temperature and stored energy in both cases for R_{ax} = 3.75 m are clear, but the clamping effect is weak as compared with those for R_{ax} = 3.6 m. The difference of clamping effect for both cases needs to be analyzed more in detail, but it is clear from the comparison with R_{ax}=3.60 m configuration that the density clamping is strongly related to the magnetic ripple rate at the heating region, implying that the ECRH related physics plays an important role in the clamping phenomena.

In Fig. 6 are shown the time evolutions of the density, central electron and ion temperature in response to the ECRH on NB heated plasma for ripple top and bottom resonance heating conditions. In both cases, density decrease is observed by applying ECRH, but the time behavior of the decrease in the density clearly changes as the heating position. The line averaged density decreases faster in ripple bottom heating case than in top one. The decrease rate saturates in the time constant of 200 ms for the bottom heating case, while that for the top heating case keeps constant during the ECRH injection of 500 ms. Electron temperature increases within 100 ms and keeps almost constant during the injection for both cases. The profile changes of density reconstructed from a multi-chord FIR interferometer are shown in Fig.7. It should be noted that the density drops at $\rho > 0.4$ but central part does not affected by the ECRH injection for top heating case, while that drops almost whole region for bottom heating case. The electron temperature profile changes within 0.1 s and kept almost constant during ECRH pulse for both cases.

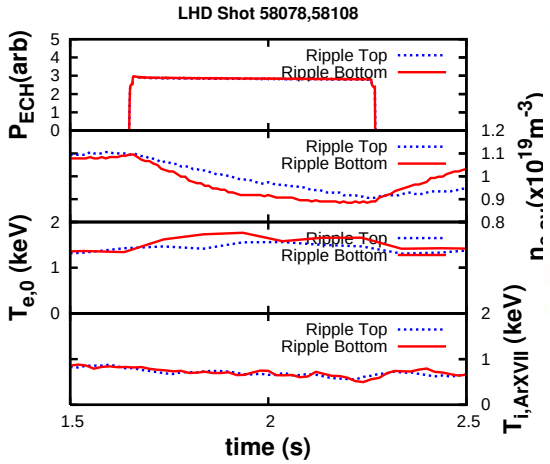

Figure 6: *Temporal evolutions of line averaged density, central electron and ion temperature for ripple top (dotted lines) and bottom (thick lines) ECRH on NB heated discharge.*

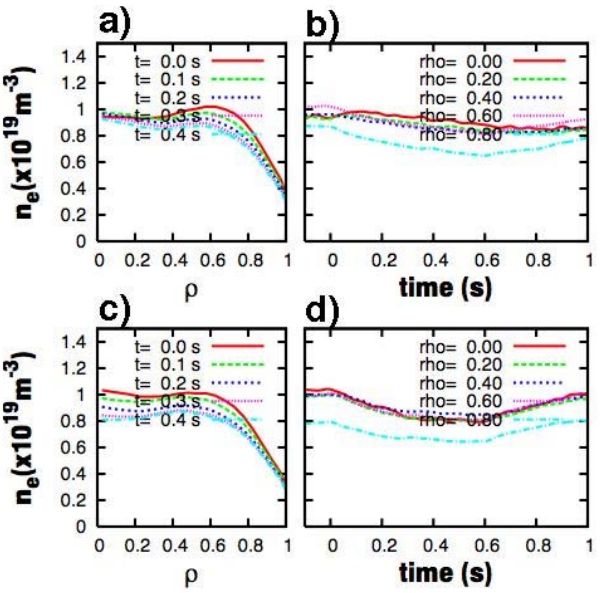

Figure 7: *Density profile at several time slices after ECH injection [a) and c)]. Time evolutions of the density at several spatial points b), and d) for ripple top [a) and b)] and bottom [c)and d)] heating cases.*

The temperature increase of the central region for the case of ripple bottom due to the ECRH is larger as compared with the ripple top case. In both cases, the profile change occurs in less than 100 ms and kept almost constant after 100 ms from the ECRH injection. This means that the change in the density profile evolutions after 100 ms of ECRH injection are attributed to the diagonal term and direct flux due to the ECRH in the electron diffusion.

Neglecting the source and sink term other than that due to ECRH, diffusion equation can be written by electron density $n_e(r,t)$and temperature profiles $T_e(r,t)$ as

$$\Gamma_e(r,t) = D_{e,n}(r,t)\frac{\partial n_e(r,t)}{\partial r} + D_{e,T}(r,t)\frac{\partial T_e(r,t)}{\partial r} + \Gamma_{ECH}(r,t). \quad (1)$$

Here, $D_{e,n}(r,t)$ denotes the normal electron diffusion coefficient, while $D_{e,T}(r,t)$ does an off-diagonal element due to electron temperature gradient. Then, the diffusion equation is expressed with this electron flux $\Gamma_e(r,t)$ as

$$\frac{\partial n_e(r,t)}{\partial t} = -\frac{\partial}{r\partial r}\Big(r\Gamma_e(r,t)\Big). \quad (2)$$

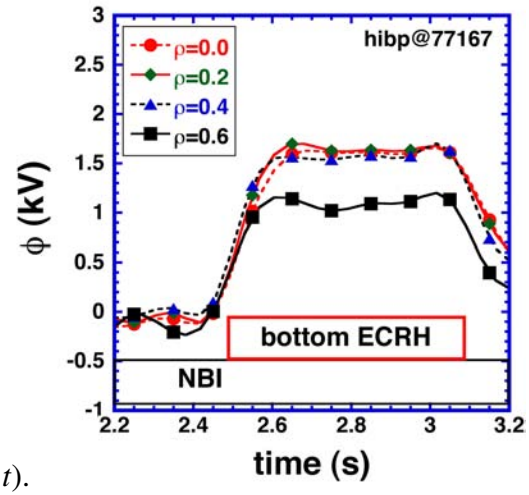

Figure 8: *Potential change during density pump out experiment measured by heavy ion beam probe at rho=0.0, 0.2, 0.4 and 0.6. Positive potential is formed as the ECRH turned on and strong radial electric field is observed near the resonance position at ρ=0.3 for the ripple bottom heating case.*

Integrating over radius of Eq. (2) gives

$$\Gamma_e(r,t) = -\frac{1}{r}\int_0^r r' \frac{\partial n_e(r',t)}{\partial t} \mathrm{d}r'. \quad (3)$$

Thus total electron flux can be deduced from Eq. (3) by the experimentally observed quantity $n_e(r',t)$. Fast increase of the flux at $\rho > 0.3$ is clear in the ripple bottom heating case than that in the top case. As is expected from Eq. (1), the correlations between density profile change and flux change indicate the effect of normal diffusion coefficient, but there seems no clear correlation between them. Second term in Eq. (1) describes the off-diagonal term from the temperature gradient.

As is described above, the temperature profile change occurs only at the beginning 100 ms after ECRH injection for both cases. So the correlation between the deduced flux and the temperature gradient should also be weak. These results indicate that the change in the deduced particle flux for the ripple top and bottom cases are directly driven by ECRH, although the dynamical dependence of the diffusion coefficient on the temperature and its gradient, off-diagonal term and the effect of the radial electric field should be considered more carefully.

The dynamics of the electric field and ECRH induced particle flux are investigated using heavy ion beam probe as shown in Fig. 8. Here, the ECRH power of 200 kW is concentrated at the ripple bottom near $\rho = 0.3 \pm 0.02$. The temperature profile changes within the time scale of 80 ms, while the potential profile change takes more than 100 ms as shown in Fig. 8. The time scale of density profile response is more than 300 ms. The comparison of the density, temperature, and potential profile change could clarify the dynamics of the direct ECRH induced radial flux and positive radial electric field toward the outside of the deposition region.

5 Current profile control

Local power deposition is also powerful tool for driving local current to control the current profile. The advantage of the ECCD in helical system is that the current drive physics appears directly to the change in the rotational transform, due to the lack of ohmic current. Change in the rotational transform successfully measured by MSE for co and counter ECCD are shown in Fig. 9 a). The driven current of the order of 10 kA is localized near the center and directed as expected from Fisch-Boozer theory.

Driven current density profile estimated from these temporal changes in the rotational transform are shown in Fig. 9 b). Driven current is concentrated less than $\rho < 0.4$ and the transient reverse current compensates outside resulting in total measured current outside in few kA.
The power deposition region expected from raytracing calculation is within $\rho = 0.2$ for all cases. The width of the deposition region tends to be equally large for the co- and counter ECCD cases as compared with ECRH case, due to the Doppler effect. Asymmetry in the driven current on drive direction might indicate the dynamic change in the ECCD efficiency due to the change of rotational transform.

6 Conclusion

Highly focused and well defined power deposition is realized in LHD. This feature of the ECRH is applied to achieve and investigate ECRH and ECCD of high electron temperature plasma. Power deposition profile achieved is confirmed by the direct beam profile measurement inside the vacuum vessel. Experimental power deposition profile deduced from the modulation

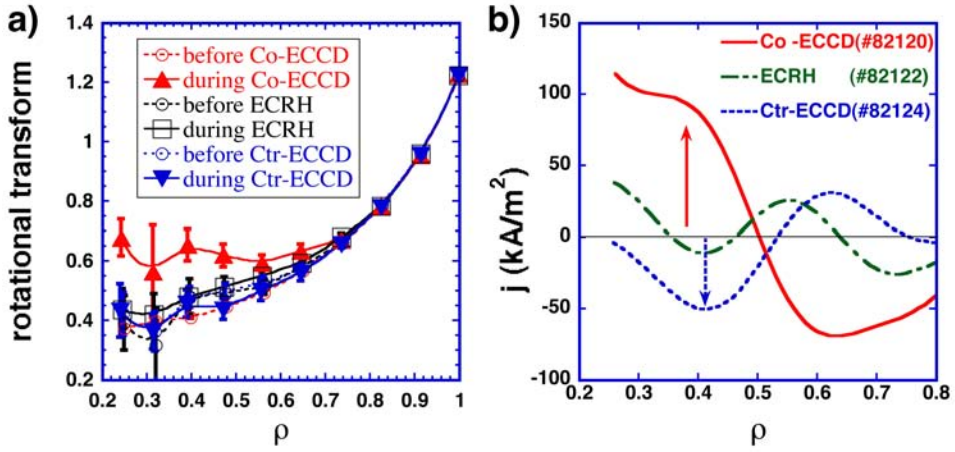

Figure 9: *a) Rotational transform measured by MSE before and during Co-, Ctr- ECCD and ECRH. b) Driven current density estimated from the difference of the rotational transform in a) for Co- (thick line) Ctr- (dashed line) ECCD and ECRH (dash dotted line).*

experiment also indicate the well controlled and coincide well with the results of ray tracing calculation. It is also clarified that high energy electrons are created and localized near the magnetic axis in low density discharge.

With these well defined power deposition profile and controllability, density and current profile control are performed and detailed diagnostics including HIBP and MSE confirmed the local profile control effects.

[1] S. Kubo, *et al. Plasma Physics and Controlled Fusion*, **47** 5A (2005) A81.

[2] T. Shimozuma, S. Kubo, H. Idei, Y. Yoshimura, *et al.*, *Plasma Physics and Controlled Fusion*, **45** (2003) 1183.

[3] S. Kubo *et al.*, J. Plasma Fusion Res. SERIES **5**, (2002) 584.

[4] G. Bekefi, *Radiation Processes in Plasma*, John Wiley & Sons Inc., New York, (1966).

[5] N. Marushchenko *et al.*, Plasma and Fusion Research, **2**, (2007) S1129.

[6] S. Kubo, *et al. Proc. 33rd EPS Conference on Plasma Phys. Rome, 19 - 23 June 2006 ECA* **Vol.30I**, (2006) P-4.116.

[7] K. Itoh *et al.*, J. Phys. Soc. Japan **58**, (1989) 482.

[8] H. Sanuki *et al.*, Phys. Fluids, **B2**, (1990) 2155.

[9] H. Idei *et al.*, Fusion Engineering and Design **26**, (1995) 167.

[10] C. Angioni *et al.*, Nuclear Fusion **44**, (2004) 167.